Carbohydrate Polymers 101 (2014) 614–622

Contents lists available at ScienceDirect

Carbohydrate Polymers

journal homepage: www.elsevier.com/locate/carbpol

Telmisartan complex augments solubility, dissolution and drug delivery in prostate cancer cells

Manveet Kaur[a], Richa Kaur Bhatia[a], Raghuvir R.S. Pissurlenkar[b], Evans C. Coutinho[b], Upendra Kumar Jain[a], Om Prakash Katare[c], Ramesh Chandra[d], Jitender Madan[a,*]

[a] Department of Pharmaceutics, Chandigarh College of Pharmacy, Mohali, Punjab, India
[b] Molecular Simulations Group, Department of Pharmaceutical Chemistry, Bombay College of Pharmacy, Mumbai, India
[c] University Institute of Pharmaceutical Sciences, Panjab University, Chandigarh, India
[d] Dr. B.R. Ambedkar Centre for Biomedical Research, University of Delhi, Delhi, India

ARTICLE INFO

Article history:
Received 19 July 2013
Received in revised form 5 September 2013
Accepted 23 September 2013
Available online 30 September 2013

Keywords:
Telmisartan
2-HP-β-CD
Complex
In silico docking
Solubility
Cytotoxicity

ABSTRACT

Telmisartan (TEL) requires superior bioavailability in cancer cell compartments. To meet these challenges, we have synthesized a 2-HP-β-CD-TEL complex with stability constant (K_c) of 2.39×10^{-3} mM. The absence in the FTIR spectrum of 2-HP-β-CD-TEL complex of the characteristic peaks of TEL at 1699 cm^{-1} (carboxylic acid) and 741 and 756 cm^{-1} (1,2-disubstituted benzene ring vibrations), is indicative of the encapsulation of TEL in the 2-HP-β-CD cavity. DSC and PXRD also confirmed the synthesis and amorphous structure of complex. The interaction of TEL with 2-HP-β-CD was examined by NMR and 2D-ROESY which affirms the encapsulation of TEL in the 2-HP-β-CD cavity in at least two orientations with equal binding energies. The complex also exhibited its superiority in both *in vitro* release and cytotoxicity experiments on prostate cancer, PC-3 cells as compared to free drug. These data warrant an in depth *in vivo* to scale-up the technology for the management of prostate cancer.

1. Introduction

It is known that 70% of all new chemical entities entering drug discovery programs are not sufficiently soluble in physiological medium to allow consistent gastrointestinal absorption of high magnitude to ensure further pharmacodynamic activities. The solubility of a drug in gastrointestinal tract is governed by multiple factors and is inherently a complex phenomenon often resulting in erratic absorption of poorly soluble drugs. Therefore, an improvement in the dissolution rate of the drug is thought to be a key factor for improving the pharmacokinetic and pharmacodynamic activities. Nanonization of lipophilic drugs by methods such as crystal modification, size reduction, pH modification and amorphization have been reported to enhance solubility and thereby bioavailability of drugs (Jain et al., 2013). Thus, *state-of-the-art* nanonization techniques much earlier in the drug discovery and development cascade are warranted to increase the number of therapeutic agents available for clinical studies.

Angiotensin II receptor blockers (ARBs) have been categorized as antihypertensive agents (Billecke & Marcovitz, 2013). In addition, ARBs have the potential to inhibit the growth of several types of cancer cells (Abali et al., 2002). Telmisartan (TEL), a component in the armamentarium of ARBs inhibits 12-O-tetradecanoylphorbor-13-acetate (TPA)-induced cell proliferation stronger than candesartan (Ozeki et al., 2013). TEL has peroxisome proliferator-activated receptor (PPAR)-γ activation activity. It causes significant growth inhibition in the prostate cancer cells in a dose- and time-dependent manner (Matsuyama et al., 2010). Thus, TEL could be a new potent chemical entity for the prevention and treatment of human cancers. However, poor aqueous solubility (0.078 mg/ml) and suboptimal oral bioavailability (>50%) (Marasini et al., 2013; Stangier et al., 2000) consequently appeal for development of a clinically viable oral dosage form which can offer superior pharmacokinetic profile and high therapeutic concentration in cancer cell compartments.

We have successfully synthesized cyclodextrin (CDs) complexes of anticancer drugs and reported high therapeutic index in human cancer cells (Chauhan et al., 2013; Madan et al., 2010, 2012). Biocompatible CDs have been approved by Food and Drug Administration for human consumption. CDs have bucket shaped structures which enable pharmaceutical scientists to entrap a wide variety of lipophilic drugs (Sangalli et al., 2001). Structurally, CDs

* Corresponding author at: Department of Pharmaceutics, Chandigarh College of Pharmacy, Mohali 140307, Punjab, India. Tel.: +91 172 3984209; fax: +91 172 3984209.
E-mail address: jitenderpharmacy@gmail.com (J. Madan).

0144-8617/$ – see front matter © 2013 Elsevier Ltd. All rights reserved.
http://dx.doi.org/10.1016/j.carbpol.2013.09.077

consisting of six, seven, or eight glucopyranose units, namely, α-, β-, and γ-CD, covalently linked by α,1-4-glycosidic bonds to form the macromolecule (Davis & Brewster, 2004). The unique properties of β-CD allow it to form a complex with a wide variety of drugs by various forces of attraction. However, the limited solubility of β-CD in the aqueous phase (18.5 mg/ml) hampers its applications in drug delivery (Stella & Rajewski, 1997). In addition, the rigid β-CD structure is acquiescent to crystallization upon complexation. However, 2-hydroxypropyl-β-cyclodextrin (2-HP-β-CD), a β-CD analog modified with a 2-hydroxypropyl unit is known to produce more wettable amorphous compounds with expanded water solubility and complexing power (Kim, 2013). 2-HP-β-CD tenders a significant advantage over β-CD as its solubility in the aqueous phase is >500 mg/ml (Lin, Chean, Ng, & Chan, 2000).

Thus, to improve the physicochemical and pharmacodynamic characteristics of TEL, we have synthesized a 2-HP-β-CD-TEL complex using inclusion chemistry via the cycloencapsulation mode. The 2-HP-β-CD-TEL complex was characterized both in solution and solid state by phase solubility analysis, Fourier-transform infrared (FTIR) spectroscopy, differential scanning calorimetry (DSC), powder X-ray diffraction (PXRD), scanning electron microscopy (SEM), and 1D/2D NMR (ROESY) spectroscopy. Also the 2-HP-β-CD-TEL complex was modeled by *in silico* docking and molecular dynamics simulations to decipher the binding poses and to estimate the relative binding affinities. Further 2-HP-β-CD-TEL complex was examined for cytotoxic activity in prostate cancer, PC-3 cells. Standard colorimetry based MTT [3-(4,5-dimethylthiazol-2-yl)-2,5-diphenyltetrazolium bromide] cell proliferation assays was used to assess the delivery and pharmacodynamic efficacy in prostate cancer cells of the complex compared to the free drug.

2. Materials and methods

2.1. Materials

Telmisartan (TEL, molecular weight ~514 Da, purity ~98%) was a gift sample from Glenmark Pharmaceuticals, India. 2-Hydroxypropyl-betacyclodextrin (2-HP-β-CD, molecular weight ~1541.54 Da) was purchased from Chemsworth, Surat, India. D_2O (99.9% purity) and dimethyl sulfoxide-d_6 (DMSO-d_6) (D, 99.9% + 1%, v/v TMS) were purchased from Cambridge Isotope Laboratories, Inc. NaOD (40 wt% in D_2O, 99+ atom% D) was purchased from Acros Organic. All other chemicals used were of highest analytical grade and used without further purification.

2.2. Cell culture

Human prostate cancer cell line (PC-3) was maintained in 5% CO_2 and 95% air at 37 °C using Dulbecco's modified Eagle's medium (DMEM) (Biologicals, Israel) supplemented with 5% fetal calf serum. All experiments were performed with asynchronous populations in exponential growth phase (24 h after plating) (Li & Sarkar, 2002).

2.3. Phase solubility analysis

Phase solubility assay was implemented to assess the stoichiometry of the 2-HP-β-CD-TEL complex in the aqueous phase (de Melo, Grillo, Rosa, & Fraceto, 2008). Briefly, TEL (20 mg) was suspended separately in 10 ml of phosphate buffer saline (PBS, pH ~7.4) containing 2-HP-β-CD at concentrations ranging from 2 to 32 mM. Next, samples were stirred in an orbital shaker (150 rpm) for five consecutive days at 37 ± 1 °C. After equilibration, the samples were passed separately through a 0.22-μm membrane filter (MDI, India), and the absorbance was read at 298 nm using an UV/visible spectrophotometer (Shimadzu, Kyoto, Japan) (Kondawar, Kamble, Raut, & Maharshi, 2011). The apparent stability constant was calculated from the slope of the phase-solubility diagram using Eq. (1):

$$K_c = \frac{\text{slope}}{S_o(1 - \text{slope})} \quad (1)$$

where K_c is the apparent binding/stability constant and S_o is the solubility of the drug in the absence of cyclodextrin.

2.4. Synthesis of solid complexes using inclusion chemistry

Solid complex of TEL with 2-HP-β-CD was synthesized by mixing TEL with 2-HP-β-CD in aqueous phase (pH ~10.0) in 1:1 molar ratio. The resultant solutions were stirred for 24 h in an orbit shaker (150 rpm) at 37 ± 1 °C. Subsequently, the solutions were lyophilized and collected as solid complex. We also prepared physical mixture of TEL with 2-HP-β-CD in a 1:1 molar ratio by mixing the individual components and passing them through sieve #100.

2.5. Characterization of solid complexes

2.5.1. Fourier-transform infrared (FTIR) spectroscopy

The first characterization of the complex of TEL with 2-HP-β-CD was done using FTIR spectroscopy. The spectra of TEL, 2-HP-β-CD, the physical mixture of TEL with 2-HP-β-CD and the complex, 2-HP-β-CD-TEL were recorded in a Perkin Elmer IR spectrophotometer. KBr was used to prepare the sample pellet (2 mg sample/200 mg KBr) at a force of 40 psi for 4 min using a hydrostatic press. The samples were scanned between 4000 and 400 cm^{-1} with a resolution of 4 cm^{-1}.

2.5.2. Differential scanning calorimetry (DSC)

DSC was used to confirm the synthesis of the complex in the solid state. Characteristic endothermic peaks of TEL, 2-HP-β-CD, physical mixture of TEL with 2-HP-β-CD and the complex, 2-HP-β-CD-TEL were recorded using a Mettler-Toledo differential scanning calorimeter. Nitrogen was used as the carrier gas at a flow rate of 45 ml/min. Thermograms were recorded at a heating rate of 20 °C/min in the temperature range of 30–300 °C with 10 mg of sample.

2.5.3. Powder X-ray diffraction pattern (PXRD)

The crystalline configuration of TEL, 2-HP-β-CD, physical mixtures of TEL with 2-HP-β-CD and the complex, 2-HP-β-CD-TEL were studied using a Rigaku, Rotaflex, RV 200 (Rigaku Corporation, Japan) X-ray diffractometer with Ni filtered, Cu Kα radiation, at a voltage of 60 kV and a current of 45 mA. The scanning rate employed was 2°/min over the diffraction angle (2θ) range.

2.5.4. Scanning electron microscopy (SEM)

TEL, 2-HP-β-CD, the physical mixture of TEL with 2-HP-β-CD and the 2-HP-β-CD-TEL complex were examined by a scanning electron microscope (SEM) to visualize the surface topography. Samples were prepared by preparing the film on an aluminum stub. The stubs were then coated with gold to a thickness of 200–500 Å under an argon atmosphere using a gold sputter module in a high vacuum evaporator. The coated samples were scanned, and photographs were taken with a SEM (Jeol-1761, Cambridge, UK) camera.

2.5.5. Nuclear magnetic resonance (^{1}H NMR) spectroscopy

^{1}H NMR spectra were recorded on a Bruker DPX 300 MHz spectrometer to analyze the chemistry of the complex. The solution of TEL (6.0 mM) was prepared in deuterated dimethyl sulfoxide (DMSO-d_6) while 2-HP-β-CD-TEL complex and 2-HP-β-CD (6.0 mM) were prepared separately in deuterated water (D_2O) and then transferred to NMR tubes. The probe temperature was

set at 293 K. The ^{1}H NMR spectra were recorded using a simple pulse-acquire sequence (zg30). Typical acquisition parameters were 64 transients, 3.16 kHz spectral window, a 60° pulse angle giving a digital resolution of 0.048 Hz/point, and a 10.4 s acquisition time with relaxation delay of 1.0 s. ^{1}H chemical shifts in D_2O solutions were referenced against sodium 4,4-dimethyl-4-silapentanesulfonate (DSS) with a coaxial inner tube containing 60 μL of 5.0 mM DSS in D_2O. DSS was not used internally to avoid possible interaction with the 2-HP-β-CD. For DMSO-d_6 solutions, TMS (tetramethylsilane) was used as an internal reference. 2D rotating frame Overhauser effect correlation (ROESY) spectra were recorded with a sweep width of 8.5 ppm in both dimensions. The ROESY mixing time was set to 150 ms. The spectrum was acquired with 32 scans, 2048 data points in t2, and 512 free induced decays (FIDs) in t1. The data were apodized with a shifted sine-bell square function in both dimensions and processed to a 2×1 K matrix. ROESY data were processed and plotted using Bruker Top Spin v1.3 software. All other NMR data were processed using MestReNova v5.30 for Windows and plotted using Origin 7. Experiments were carried out at 25 ± 1 °C. The pH values of the D_2O solutions were measured at 25 °C using an Orion 720Aplus pH meter calibrated with three buffers of pH 4.0, 7.0, and 10. The pH of the D_2O solutions was adjusted using NaOD/DCl solutions in D_2O.

2.5.6. In silico docking studies

The computational studies were done on an Intel Xeon based 11-node high performance computing cluster (HCL Infosystems Limited, India) operating on the Rocks Cluster Suite 6.1. The 3D structure for β-CD was retrieved from the *Protein Data Bank* (Berman et al., 2000) and modified by alkylating appropriate hydroxyl groups to obtain 2-HP-β-CD. The molecular structures were optimized for docking using the *Schrodinger Suite 2012* (Schrodinger LLC, New York, NY, 2012) wherein the atoms types and corresponding partial charges were defined with the OLPS 2005 force field. The docking studies were performed with *FRED* v2.2.5 (Open Eye Scientific Software, Santa Fe, USA) (McGann, Almond, Nicholls, Grant, & Brown, 2003; McGaughey et al., 2007). The binding site for docking in the cavity of 2-HP-β-CD was defined by a grid box where TEL is expected to bind in a manner reported in previous publications (Chadha et al., 2011a, 2011b; Chadha, Gupta, Pissurlenkar, & Coutinho, 2012). The docking poses were obtained by scanning the rotational and translational space with the "rigid conformation" of TEL within the grid box created within the 2-HP-β-CD structure. Docking poses of TEL were scored with the *ChemGauss3* scoring function. Selected poses of TEL in complex with 2-HP-β-CD were considered for calculation of binding energy using MD simulations with *Desmond* v3.1 (DE Shaw Research, NY, 2012). Each drug-CD complex was centered in an octahedral cell and soaked with TIP3P waters (Mark & Nilsson, 2001) such that a10 Å water shell was formed around the complex. These solvated complexes were relaxed with restrains on the solute and subsequently equilibrated at 300 K and 1 atm pressure over NVT and NPT *ensembles*. After this the equilibrated system was simulated for 10 ns using the NPT *ensemble* to obtain the energy and trajectory profile of the complex from which the free energy of binding was calculated. The structural states and corresponding energies were sampled from the trajectories every 10 ps.

2.5.7. Determination of solubility

The solubility of TEL and 2-HP-β-CD-TEL complex in aqueous phase was determined by preparing the respective saturated solutions. Briefly, 20 mg of TEL was added to 1 ml of PBS (pH ~7.4) and stirred for 24 h in an orbital shaker at 37 ± 1 °C. Subsequently the suspensions were centrifuged, and supernatants were filtered through a 0.22-μm membrane filter (MDI, India) and analyzed in an UV/Visible spectrophotometer (Shimadzu, Kyoto, Japan) at 298 nm (Kondawar et al., 2011). A similar method was followed for the complex of TEL with 2-HP-β-CD. All experiments were carried out in triplicate ($n \geq 3$).

2.5.8. In vitro dissolution testing

Dissolution studies were conducted as per the standard protocol using USP dissolution rate test type II apparatus (Bai, Wang, & Armenante, 2011). The dissolution study of TEL and 2-HP-β-CD-TEL complex equivalent to 40 mg of drug was carried out in 900 ml of simulated intestinal fluid (SIF) maintained at 37 °C. The dissolution medium was stirred at 50 rpm (as recommended for dissolution testing of oral products) (Anand, Yu, Conner, & Davit, 2011). A 5 ml sample was withdrawn at 1, 5, 10, 15, 30, 45, 60 and 120 min, and an equivalent amount of fresh SIF (pH ~7.4) was added to mimic sink conditions. The TEL concentration was determined using an UV/Visible spectrophotometer (Shimadzu, Kyoto, Japan) at 298 nm (Kondawar et al., 2011). The experiment was carried out in triplicate ($n \geq 3$).

2.5.9. In vitro cytotoxicity assay

MTT [3-(4,5-dimethylthiazol-2-yl)-2,5-diphenyltetrazolium bromide] assay was used to determine the cytotoxicity of TEL and 2-HP-β-CD-TEL complex using 96 well microtitre plates (Mosmann, 1983). Briefly, 5×10^3 PC-3 cells were placed in 200 μL of the serum DMEM. The medium was replaced with serum free-DMEM after 24 h of incubation period. Subsequently seeded cells were incubated with a gradient concentration of TEL, 2-HP-β-CD-TEL complex and 2-HP-β-CD equivalent to TEL concentration of 20–100 μM for 72 h. After the predetermined incubation period, MTT (0.5 mg/ml) was added and the plate was incubated for 4 h at 37 °C. The formazon crystals formed after cell lyses were dissolved using 100 μL of DMSO. The absorbance was read at 570 nm using 630 nm as reference (Tecan, Switzerland).

2.6. Statistical analysis

The statistical significance of all assays was analyzed with one-way analysis of variance and Student's t test. $P < 0.05$ was taken as a significant level of difference. The results are presented as mean ± SD for $n \geq 3$.

3. Results

3.1. Phase solubility analysis

The main aim of the present investigation was to explore the ability of 2-HP-β-CD to potentiate the therapeutic index of TEL in cancer chemotherapy by improving its solubility and dissolution characteristics (Matsuyama et al., 2010; Ozeki et al., 2013). In this study we have invoked the power of inclusion chemistry to stabilize and solubilize TEL via the lyophilization-based cycloencapsulation technique. To this end, our first step was to determine the composition, stoichiometry, and the apparent stability constant (K_c) of this complex. To accomplish this we employed phase solubility analysis using a gradient concentration of 2-HP-β-CD in solution phase as per the Higuchi and Connors system (Higuchi & Connors, 1956). The phase-solubility diagram of the complex of TEL with 2-HP-β-CD in solution state is shown in Fig. 1. The curve demonstrates that the solubility of TEL increases linearly as a function of concentration of 2-HP-β-CD. These data imply that the solubility diagram of TEL with 2-HP-β-CD is of the A_L type. The stability constant (K_c) of the binary system of TEL with 2-HP-β-CD is calculated to be 2.39×10^{-3} mM, from the linear plot of the phase solubility diagram.

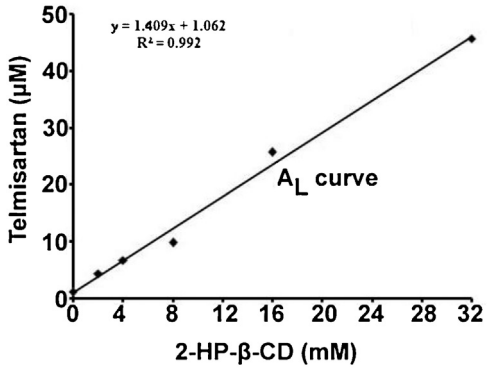

Fig. 1. Phase solubility analysis of TEL in the presence of a gradient concentration of 2-HP-β-CD (2–32 mM) in phosphate buffer saline (pH ~7.4). The solubility diagram of TEL with 2-HP-β-CD is of the A_L type and the stability constant (K_c) was calculated to be 2.39×10^{-3} mM, from the linear plot of the phase solubility diagram.

3.2. FTIR

Next, we characterized the complex of TEL with 2-HP-β-CD using FTIR in the solid state. Spectra were recorded to analyze the alteration of stretching frequencies due to hydrophobic interaction of TEL in the 2-HP-β-CD cavity (Table 1). The spectrum of TEL demonstrated the characteristic peaks at 3059 cm^{-1} (aromatic C—H stretch), 2957 cm^{-1} (aliphatic C—H stretch), 1699 cm^{-1} (carboxylic acid), 1599 cm^{-1} (aromatic C=C bending and stretching), 1459 cm^{-1} (C—H bend), 1382 cm^{-1} (—OH bending and C=O stretching of carboxylic acid), 741 and 756 cm^{-1} (1,2-disubstituted benzene ring vibrations), respectively. The FTIR spectrum of 2-HP-β-CD is characterized by intense bands at 3300–3500 cm^{-1} due to O—H stretching vibrations, a characteristic band of all CDs. The vibration of the —CH and $—CH_2$ groups appears in the 2800–3000 cm^{-1} region. The physical mixture of TEL and 2-HP-β-CD has showed characteristics band of individual components. The chemical interaction has been reflected by changes in the

Table 1
Assignment of FTIR peaks of TEL, 2-HP-β-CD, physical mixture of TEL and 2-HP-β-CD and 2-HP-β-CD-TEL complex.

Samples	Peaks	Assignment	Samples	Peaks	Assignment
Telmisartan 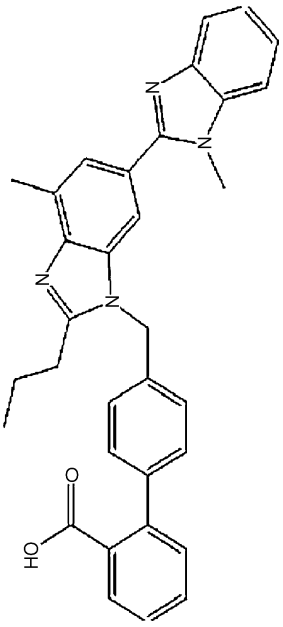	3059 cm^{-1}	(aromatic C—H stretching)	Complex	3058 cm^{-1}	(aromatic C—H stretching)
	2957 cm^{-1}	(aliphatic C=H stretching)			
	1699 cm^{-1}	(COOH stretching)		1652 cm^{-1}	(H—O—H bending)
	1599 cm^{-1}	(C—C aromatic band and stretching)		1014 cm^{-1}	(C—O—C bending)
	1459 cm^{-1}	(C—H bend)			
	1382 cm^{-1}	(—OH bending and C=O stretching of —COOH acid)			
	741 cm^{-1}	(ring vibration due to 1,2-disubstituted benzene)			
	756 cm^{-1}				
2-HP-β-CD, 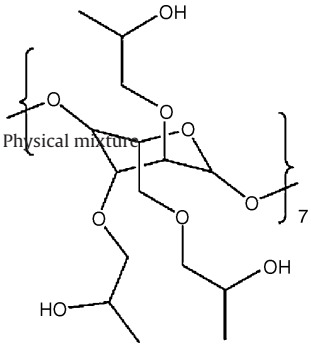	3401 cm^{-1}	(—OH stretching)			
	2928 cm^{-1}	(—CH stretching)			
	1652 cm^{-1}	(H—O—H bending)			
	1164 cm^{-1}	(C—H stretching)			
	1085 cm^{-1}	(C—O stretching)			
	1032 cm^{-1}	(C—O—C bending)			
Physical mixture	2957 cm^{-1}	(aliphatic C=H stretching)			
	2928 cm^{-1}	(—CH stretching)			
	1697 cm^{-1}	(COOH stretching)			
	1652 cm^{-1}	(H—O—H bending)			
	1014 cm^{-1}	(C—O—C bending)			

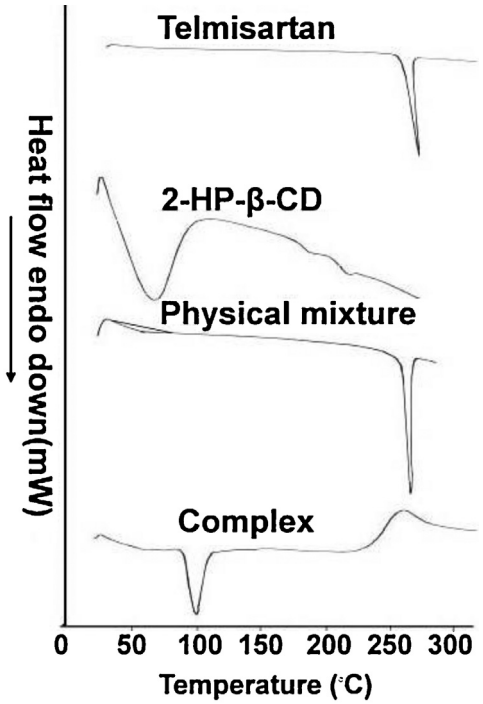

Fig. 2. Differential scanning calorimetry (DSC) analysis of TEL, 2-HP-β-CD, physical mixture of TEL and 2-HP-β-CD and 2-HP-β-CD-TEL complex. The thermogram of 2-HP-β-CD-TEL complex shows a complete disappearance of the endothermic peaks characteristic of TEL with a significant shift in the 2-HP-β-CD peak.

characteristic peaks of TEL, depending on the degree of interaction. The FTIR spectrum of 2-HP-β-CD-TEL complex showed the absence of the characteristic peak of TEL at 1699 cm^{-1} (carboxylic acid), 2957 cm^{-1} (aliphatic C—H stretch), 1382 cm^{-1} (—OH bending and —C=O stretching of carboxylic acid), 741 and 756 cm^{-1} (1,2-disubstituted benzene ring vibrations) in complex, indicating encapsulation of TEL in 2-HP-β-CD cavity. Thus, the FTIR spectra provided us with initial information on the functional groups of TEL which enters the 2-HP-β-CD cavity.

3.3. DSC

DSC was used to confirm the synthesis of the complex of TEL with 2-HP-β-CD in the solid state. The endothermic peaks of the complex and the individual components as compared in Fig. 2. The data shows an endothermic peak of TEL at 273.25 °C near to its melting point (272 °C). The thermograms of all CDs (i.e., α-, β-, γ-CDs and derivative CDs) exhibit a range of endothermic peaks broadly ranging from 40 to 150 °C (65 °C for 2-HP-β-CD) due to the dehydration process. The thermogram of the physical mixture of TEL with 2-HP-β-CD indicated the presence of identical peaks of individual components. However, the thermogram of the complex, 2-HP-β-CD-TEL shows a complete disappearance of the endothermic peaks characteristic of TEL with a significant shift in 2-HP-β-CD endothermic peaks to 101.12 °C, respectively.

3.4. PXRD

Our next step was to define the amorphous state of TEL in the complex by the PXRD technique. The XRD pattern of TEL shows intense and sharp peaks indicative of its crystalline structure (Fig. 3). Although β-CD is crystalline in nature and shows sharp peaks in the XRD pattern however the induction of the hydroxypropyl in β-CD to form 2-HP-β-CD, transforms the crystalline structure into an amorphous state with its distinctive undefined

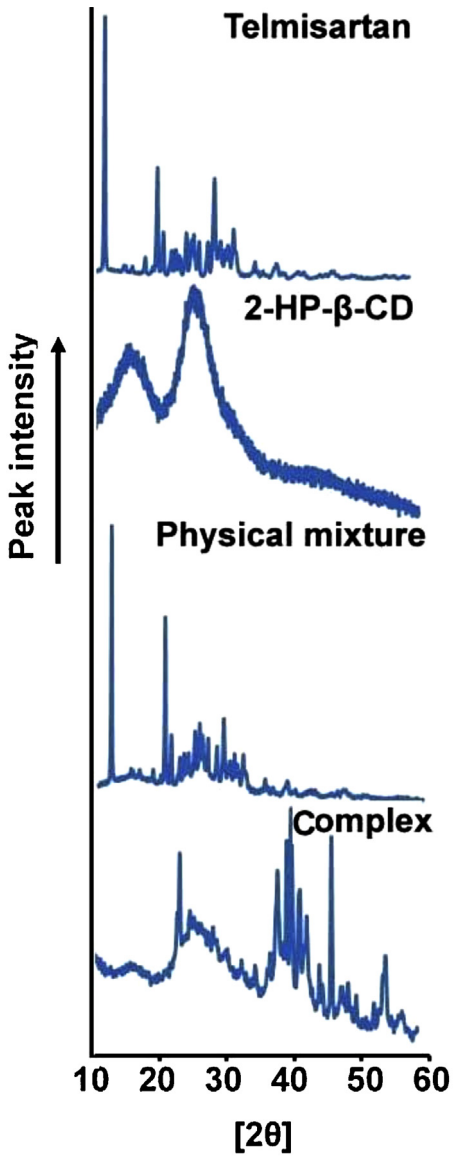

Fig. 3. Powder X-ray diffraction pattern (PXRD) of TEL, 2-HP-β-CD, physical mixture of TEL and 2-HP-β-CD and 2-HP-β-CD-TEL complex. The XRD pattern of the physical mixture of TEL with 2-HP-β-CD reveals the presence of peaks of both compounds while the 2-HP-β-CD-TEL complex shows peaks of diminished intensity with some new peaks from 35° to 60°.

broad, diffused peaks. This indicates the improved solubility of 2-HP-β-CD in water compared to β-CD. The XRD pattern of the physical mixture of TEL with 2-HP-β-CD manifests peaks of both compounds. Finally the complex of TEL with 2-HP-β-CD shows peaks of diminished intensity with some new peaks from 35° to 60°. This could be attributed to alteration in the conformational stereochemistry of TEL during the formation of complex (Rama Rao, Bhanumathi, Yadav, & Krishnaveni, 2004).

3.5. SEM

We next employed SEM to visualize the surface topography of the complex. Although this is not a confirmatory technique to assure the formation of the complex by the inclusion mode, it helps in assessment of the existence of a single component in the complex. Consistent with the results of PXRD, TEL exhibits the presence of regular size crystalline particles (Fig. 4A–D). On the contrary, 2-HP-β-CD does not show the presence of crystalline particles and

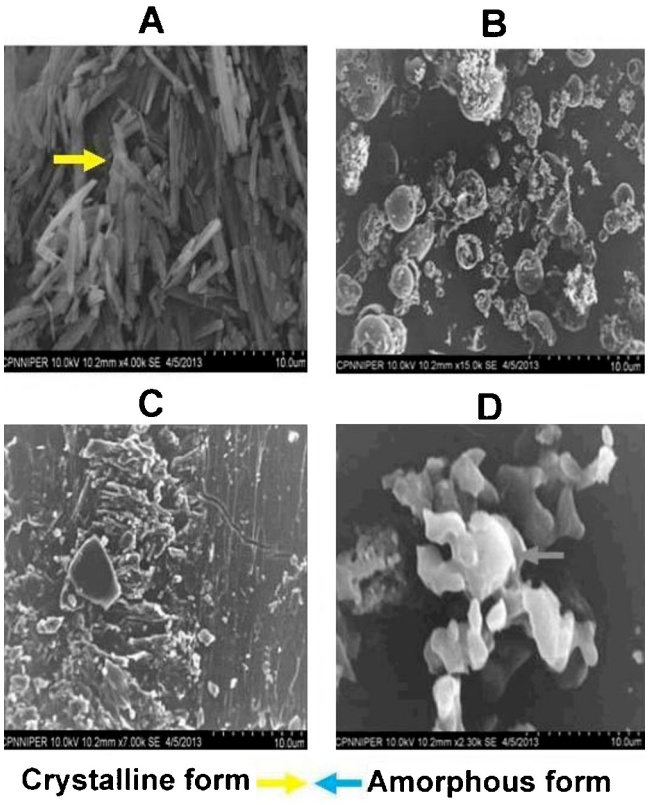

Fig. 4. Scanning electron microscopy (SEM) of (A) TEL, (B) 2-HP-β-CD, (C) physical mixture of TEL and 2-HP-β-CD, and (D) 2-HP-β-CD-TEL complex. TEL exhibits the presence of regular size crystalline particles while 2-HP-β-CD does not show the presence of crystalline particles and exists as an amorphous compound. The complex, 2-HP-β-CD-TEL assures the existence of only the amorphous product.

exists as an amorphous compound. As expected the simple physical mixture of TEL with 2-HP-β-CD shows the presence of crystalline as well as amorphous particles, whereas the complex, 2-HP-β-CD-TEL assures existences of only the amorphous product.

3.6. 1D-NMR and ROESY analysis

We next performed solution phase analysis of the complex using ^{1}H NMR spectroscopy. ^{1}H NMR provides information on the free and bound state of a host:drug complex based on the differences in the values of chemical shifts (δ). The induced chemical shift $\Delta\delta$, therefore can be defined as the difference in chemical shifts between the bound and the free guest molecule. Induced chemical shifts were calculated using the following equation: $\Delta\delta = \delta(\text{complex}) - \delta(\text{free})$. Based on this equation, positive and negative signs indicate downfield and upfield shifts, respectively. Fig. 5 shows ^{1}H NMR spectra of free 2-HP-β-CD with the respective complex in D_2O. We observed that H-1′ and H-5 protons are shifted downfield in the presence of the guest molecule, while the remaining protons (H-1, H-2, H-3, H-4, H-6, H-2′ and H-3′) are shifted upfield in the presence of TEL showing a strong interaction of TEL with 2-HP-β-CD, confirming the formation of a complex by inclusion mode (Table 2).

Additionally, 2D-ROESY experiments were used to validate through space intermolecular interactions between TEL and CD in the complex and is presented as contour plots in Fig. 5. The correlation between protons of —CH_3 and Ar—CH_2—N of TEL and the H-2, H-3, H-4, H-2′ and H-6′ protons of CD are clearly evident in the ROESY spectrum. Similarly, N—CH_3 of TEL also shows a strong correlation with the H-3′ proton of 2-HP-β-CD. These findings are consistent with the previously observed chemical shifts $\Delta\delta$. Therefore, it is appears that TEL enters the 2-HP-β-CD cavity from multiple sites and forms complexes in at least two distinct orientations.

Table 2
Chemical shifts for the protons of 2-HP-β-CD in the free-state and in complex measured using DSS as internal standard.

Proton	2-HP-β-CD (ppm)	2-HP-β-CD-TEL complex (ppm)	Status	δ (ppm)
H-1 (*d*)	5.0670	4.9969	Upfield	−0.0701
H-2 (*dd*)	3.49155	3.4536	Upfield	−0.0379
H-3 (*d*)	3.9125	3.8900	Upfield	−0.0225
H-4 (*t*)	3.3851	3.3728	Upfield	−0.0123
H-1′, H-5 (*m*)	3.62835	3.6473	Downfield	+0.01895
H-2′, H-6 (*m*)	3.7574	3.7278	Upfield	−0.0296
H-3′ (*d*)	1.0424	1.00325	Upfield	−0.03915

d: doublet, *dd*: double doublet, *t*: triplet, and *m*: multiplet.

3.7. In silico docking analysis

Docking studies revealed that TEL gets embedded in the 2-HP-β-CD cavity in two different orientations (Fig. 6). In Pose-1 the biphenyl carboxylate moiety is embedded in the cavity of 2-HP-β-CD with the N-methylbenzimidazole ring covering the secondary face of CD. In Pose-2 the reverse phenomenon is observed wherein the N-methylbenzimidazole is embedded within the CD cavity and the biphenyl carboxylate moiety is over the secondary face of 2-HP-β-CD. Hydrogen bonds between the carboxylate groups on TEL and 2-hydroxyl group on the CD molecule have a fluctuating appearance and disappearance. The free energy of binding of TEL to 2-HP-β-CD was computed over the entire MD trajectory. The complexes are seen to be stable over the entire trajectory as judged by the root mean square deviation of the 2-HP-β-CD-TEL complex. The free energy was calculated using the minimum energy structures of the complexes, the free or unbound TEL and CD molecules using Eq. (2).

$$\Delta G = K_B T \times \ln\left[\sum_{\text{minima}}^{i} \exp\left(\frac{-E_i}{K_B T}\right)\right] \quad (2)$$

Subsequently the free energy of binding was calculated using Eq. (3) as the difference between the bound and the unbound forms of TEL and 2-HP-β-CD.

$$\Delta\Delta G_{\text{binding}} = -\Delta G_{\text{complex}} + \Delta G_{\text{host}} + \Delta G_{\text{guest}} \quad (3)$$

The free energy of binding of TEL to 2-HP-β-CD is the same for the two poses, indicating that the actual situation may be a mixture of the two poses.

3.8. Determination of solubility and dissolution testing

Solubility analysis was done to ensure the effect of cycloencapsulation of TEL in 2-HP-β-CD cavity. We observed significantly ($P < 0.05$) enhanced solubility of the complex of TEL with 2-HP-β-CD (7.7 mg/ml) compared to free TEL (6.58×10^{-4} mg/ml). Thus, in quantitative terms, the solubility of TEL upon complexation with 2-HP-β-CD increases by several fold compared to the free drug. Furthermore, dissolution studies of the complex of TEL in simulated intestinal fluid (pH ~7.4) are presented as dissolution curves in Fig. 7. These data indicate that only 25% of TEL is released from the hard gelatin capsule of pure drug at 120 min compared to the TEL complex (2-HP-β-CD-TEL) which releases significantly ($P < 0.05$) higher amount 73.9% of drug in the same time interval.

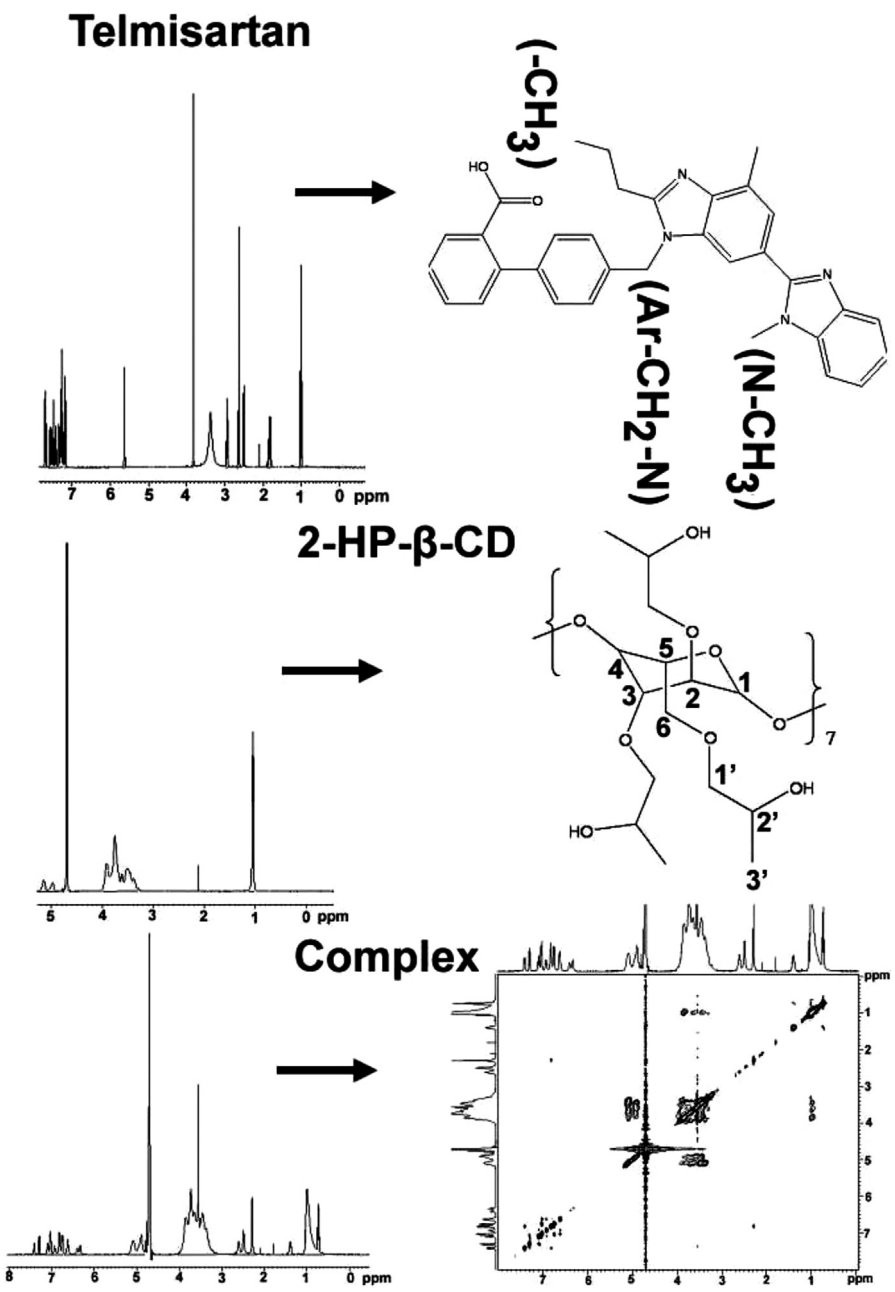

Fig. 5. ^{1}H NMR spectrum of TEL, 2-HP-β-CD and ^{1}H NMR and 2D-NMR (ROESY) of 2-HP-β-CD-TEL complex. The correlation between protons of —CH_3 and Ar—CH_2—N of TEL and H-2, H-3, H-4, H-2′ and H-6′ has been shown. Similarly, N—CH_3 of TEL also shows correlation with the H-3′ proton of 2-HP-β-CD. It appears that TEL enters the 2-HP-β-CD cavity from multiple sites and favors the formation of complex in multiple orientations.

3.9. *In vitro* cytotoxicity

In vitro cytotoxicity analysis was done to analyze the therapeutic efficacy of the complex of TEL with 2-HP-β-CD in human prostate cancer cells (PC-3) by dissolving the formulations in phosphate buffer saline (pH ~7.4). The cytotoxic activity was evaluated using the standard MTT cell viability assay. As shown in Fig. 8, the lowest IC_{50} value (31.3 μM) was observed for the complex of TEL with 2-HP-β-CD (2-HP-β-CD-TEL). However, TEL which is practically insoluble in phosphate buffer saline (pH ~7.4) shows an IC_{50} value of ~100 μM in PC-3 cells. This partly stems from its poor solubility. This was significantly ($P < 0.05$) higher than the complex of TEL.

4. Discussion

Angiotensin receptor blockers (ARBs) have been classified as antihypertensive agents from the 1990s. Recently, angiotensin II has been reported to promote tumor growth and angiogenesis (Huang et al., 2008). Hence, ARBs have been considered as promising anti-angiogenesis anticancer agents and this warrants detailed exploration as a future therapeutic option. Human cancer cells such as melanoma, pancreatic, breast and prostate show overexpression of angiotensin II receptors and making ARBs as new potential chemotherapeutic agents for cancer and related diseases (Fujimoto, Sasaki, Tsuchida, & Chayama, 2001; Goldfarb, Diz, Tubbs, Ferrario, & Novick, 1994; Inwang et al., 1997; Kosaka et al., 2007; Kosugi,

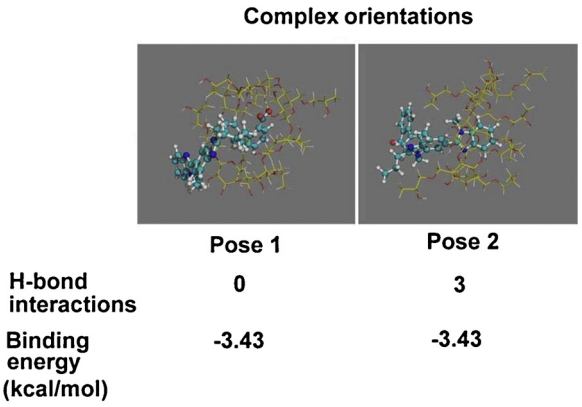

Fig. 6. *In silico* docking of 2-HP-β-CD-TEL complex and binding energies. The free energy of binding of TEL to 2-HP-β-CD is the same for the two poses, indicating that the actual situation may be a mixture of the two poses.

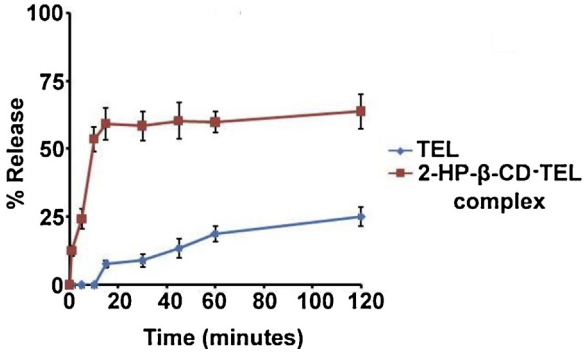

Fig. 7. *In vitro* dissolution test of TEL and 2-HP-β-CD-TEL complex in simulated intestinal fluid (pH ~7.4) at 37 °C. These data indicate that only 25% of TEL is released from the hard gelatin capsule of pure drug at 120 min compared to the TEL complex (2-HP-β-CD-TEL) which releases significantly ($P < 0.05$) higher 73.9% drug in the same time interval.

Miyajima, Kikuchi, Horiguchi, & Murai, 2006; Miyajima et al., 2002). TEL is one such ARB that blocks the angiotensin II receptor and also activates PPAR-γ (Benson et al., 2004). However, its lipophilic character (log *P* value ~3.2) (Wienen et al., 2000) and suboptimal physicochemical properties necessitates the development of viable formulations for its preclinical development. Therefore, in present investigation, we have made a complex of TEL with 2-HP-β-CD to facilitate aqueous solubility and improved the therapeutic index in cancer cell compartments. It has been reported that low molecular weight compounds exist in a 1:1 ratio with CD, wherein a single drug molecule is encapsulated in the hydrophobic cavity of one CD molecule, with a stability constant of $K_{1:1}$ for the equilibrium between the free and associated species (Davis & Brewster, 2004; Stella & Rajewski, 1997). The phase-solubility experiments provide evidence that TEL forms a 1:1 complex with 2-HP-β-CD in the solution state (Fig. 1). The phase-solubility diagram can be classified as A_L type showing the formation of a water-soluble complex with a suggestive first-order kinetics for the complex formation between TEL and 2-HP-β-CD. Further, various spectral techniques were employed to elucidate the structure of the complex in the solid state. FTIR spectral data showed that TEL remained stable in the complex and there is no opening of nitrogenous rings. However, the FTIR data suggests that inclusion of the drug into the CD cavity may occur in multiple binding poses (Table 1). DSC thermoanalysis confirms the formation of a 1:1 complex in the solid state as the endothermic peak of TEL disappears in the 2-HP-β-CD-TEL complex when compared with the endothermic peak of 2-HP-β-CD alone (Fig. 2). Furthermore, PXRD patterns of the complex of TEL with 2-HP-β-CD exhibits peaks of diminished intensity in comparison to the sharp peaks of TEL (Fig. 3). The PXRD spectroscopy substantiated that TEL resides in the 2-HP-β-CD cavity in a polymeric amorphous state. Typically, owing to irregular structural configurations, the amorphous phase entails minimal energy and thus offers the utmost solubility and bioavailability of drugs. In continuation with the results of PXRD, the photomicrographs of SEM also confirmed the existence of TEL in an amorphous state in 2-HP-β-CD complex (Fig. 4A–D). The above inferences were strongly supported by 1D and 2D-NMR as well as *in silico* docking studies and molecular dynamics simulations. Based on the difference in chemical shifts, ^{1}H NMR spectroscopy offers evidence of formation of the complex between the guest and host molecules. Changes in the chemical shift (δ) of several protons of TEL as a consequence of binding speak of at least two distinct binding poses with the CD cavity (Table 2 and Fig. 5). Precise orientation of the drug in the CD cavity was provided by the ROESY spectra and this was corroborated by the *in silico docking* and simulation exercises (Fig. 6). A significant enhancement of TEL solubility by several fold was effected upon complexation with 2-HP-β-CD as is evident from the dissolution profiles given in (Fig. 7). The pK_a of TEL is 4.45 ± 0.09 (Cagigal, Gonzalez, Alonso, & Jimenez, 2001). Usually, weakly acidic drugs are ionized in intestinal pH and stay undissociated at acidic pH. This suggests that TEL is readily absorbed throughout the gastrointestinal tract, except the stomach. TEL being a weakly acidic drug requires basic physiological dissolution media to dissolve and should remain in the unionized form to facilitate its absorption. We believe that TEL after incorporation into 2-HP-β-CD macrocycles has an increased solubility at intestinal pH. The dissolution data in SIF confirms increased drug dissolution upon complexation with 2-HP-β-CD as the complex releases significantly ($P < 0.05$) higher amounts of the drug compared to pure TEL. Thus after release from the complex, TEL will dissolve in the intestinal media to allow its absorption into systemic circulation. Consistent with the dissolution data, we observe that the complex of TEL with 2-HP-β-CD inhibits proliferation of PC-3 cells at lower IC_{50} compared to the free drug (Fig. 8). It is likely that the complex enhances the rate of diffusion of drug across the cell membrane since TEL is available in the soluble unionized state in PBS at pH ~7.4.

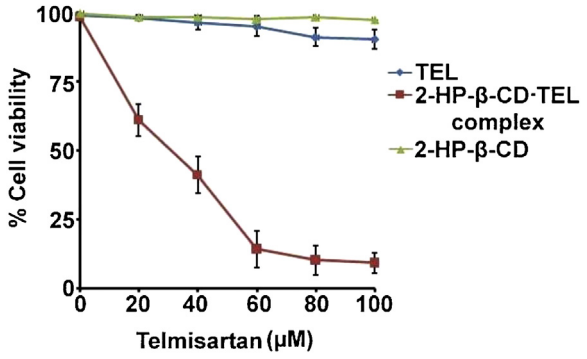

Fig. 8. *In vitro* cytotoxicity assay of TEL and 2-HP-β-CD-TEL complex carried out on PC-3, human prostate cancer cell line. TEL which is practically insoluble in phosphate buffer saline (pH ~7.4) shows an IC_{50} value of ~100 μM in PC-3 cells. This is significantly ($P < 0.05$) higher than the complex of TEL (31.3 μM).

5. Conclusions

In conclusion, the present study describes the use of FDA approved CD to enhance the solubility and cytotoxicity of TEL. Using various spectral techniques and computational studies, our data provide sufficient evidence that the CD-based complex improves the physicochemical and biological properties of TEL. These data

are encouraging and thus warrant a future in depth pre-clinical study to scale-up the technology for the management of prostate cancer.

Acknowledgements

The computational facilities supported by the Department of Biotechnology (DBT; BT/TF-8/BRB/2009) and CSIR (01/2399/10/EMRII and 02(0047)/12/EMR-II), New Delhi to Bombay College of Pharmacy, Mumbai, India are gratefully acknowledged.

References

Abali, H., Gullu, I. H., Engin, H., Haznedaroglu, I. C., Erman, M., & Tekuzman, G. (2002). Old antihypertensive as novel antineoplastics: Angiotensin-I-converting enzyme inhibitors and angiotensin II type 1 receptor antagonists. *Medical Hypotheses*, *59*, 344–348.

Anand, O., Yu, L. X., Conner, D. P., & Davit, B. M. (2011). Dissolution testing for generic drugs: An FDA perspective. *AAPS Journal*, *13*, 328–335.

Bai, G., Wang, Y., & Armenante, P. M. (2011). Velocity profiles and shear strain rate variability in the USP dissolution testing apparatus 2 at different impeller agitation speeds. *International Journal of Pharmaceutics*, *403*, 1–14.

Benson, S. C., Pershadsingh, H. A., Ho, C. I., Chittiboyina, A., Desai, P., Pravenec, M., et al. (2004). Identification of telmisartan as a unique angiotensin II receptor antagonist with selective PPARγ-modulating activity. *Hypertension*, *43*, 993–1002.

Berman, H. M., Westbrook, J., Feng, Z., Gilliland, G., Bhat, T. N., Weissig, H., et al. (2000). The protein data bank. *Nucleic Acids Research*, *28*, 235–242.

Billecke, S. S., & Marcovitz, P. A. (2013). Long-term safety and efficacy of telmisartan/amlodipine single pill combination in the treatment of hypertension. *Vascular Health Risk Management*, *9*, 95–104.

Cagigal, E., Gonzalez, L., Alonso, R. M., & Jimenez, R. M. (2001). pK_a determination of angiotensin II receptor antagonists (ARA II) by spectrofluorimetry. *Journal of Pharmaceutical and Biomedical Analysis*, *26*, 477–486.

Chadha, R., Gupta, S., Pissurlenkar, R. R. S., & Coutinho, E. C. (2012). Characterization, thermodynamic parameters, molecular modeling and *in vivo* studies of inclusion complexes of pyrimethamine with native β-cyclodextrin and its derivatives. *International Journal of Pharmaceutical Sciences*, *4*, 102–112.

Chadha, R., Gupta, S., Shukla, G., Jain, D. V. S., Pissurlenkar, R. R. S., & Coutinho, E. C. (2011a). Interaction of artesunate with β-cyclodextrins: Characterisation, thermodynamic parameters, molecular modeling, effect of PEG on complexation and antimalarial activity. *Results in Pharmaceutical Sciences*, *1*, 38–48.

Chadha, R., Gupta, S., Shukla, G., Jain, D. V. S., Pissurlenkar, R. R. S., & Coutinho, E. C. (2011b). Binary and ternary complexes of arteether β-CD-characterization, molecular modeling and *in vivo* studies. *Pharmacology and Pharmacy*, *2*, 212–225.

Chauhan, R., Madan, J., Kaushik, D., Sardana, S., Pandey, R. S., & Sharma, R. (2013). Inclusion complex of colchicine in hydroxypropyl-β-cyclodextrin tenders better solubility and improved pharmacokinetics. *Pharmaceutical Development and Technology*, *18*, 313–322.

Davis, M. E., & Brewster, M. E. (2004). Cyclodextrin-based pharmaceutics: Past, present and future. *Nature Reviews Drug Discovery*, *3*, 1023–1035.

de Melo, N. F., Grillo, R., Rosa, A. H., & Fraceto, L. F. (2008). Interaction between nitroheterocyclic compounds with beta-cyclodextrins: Phase solubility and HPLC studies. *Journal of Pharmaceutical and Biomedical Analysis*, *47*, 865–869.

Fujimoto, Y., Sasaki, T., Tsuchida, A., & Chayama, K. (2001). Angiotensin II type 1 receptor expression in human pancreatic cancer and growth inhibition by angiotensin II type 1 receptor antagonist. *FEBS Letters*, *495*, 197–200.

Goldfarb, D. A., Diz, D. I., Tubbs, R. R., Ferrario, C. M., & Novick, A. C. (1994). Angiotensin II receptor subtypes in the human renal cortex and renal cell carcinoma. *Journal of Urology*, *151*, 208–213.

Higuchi, T., & Connors, A. K. (1956). Advances in analytical chemistry and instrumentation. *Advances in Analytical Chemistry and Instrumentation*, *4*, 117–212.

Huang, W., Wu, Y. L., Zhong, J., Jiang, F. X., Tian, X. L., & Yu, L. F. (2008). Angiotensin II type 1 receptor antagonist suppress angiogenesis and growth of gastric cancer xenografts. *Digestive Diseases and Science*, *53*, 1206–1210.

Inwang, E. R., Puddefoot, J. R., Brown, C. L., Goode, A. W., Marsigliante, S., Ho, M. M., et al. (1997). Angiotensin II type 1 receptor expression in human breast tissues. *British Journal of Cancer*, *75*, 1279–1283.

Jain, V., Jain, B., Tiwari, P., Saini, J., Jain, U. K., Pandey, R. S., et al. (2013). Nanosolvated microtubule-modulating chemotherapeutics: A case-to-case study. *Anticancer Drugs*, *24*, 327–336.

Kim, M. S. (2013). Influence of hydrophilic additives on the supersaturation and bioavailability of dutasteride-loaded hydroxypropyl-β-cyclodextrin nanostructures. *International Journal of Nanomedicine*, *8*, 2029–2039.

Kondawar, M. S., Kamble, K. G., Raut, K. S., & Maharshi, K. H. (2011). UV spectrophotometric estimation of amlodipine besylate and telmisartan in bulk drug and dosage form by multiwavelength analysis. *International Journal of ChemTech Research*, *3*, 1274–1278.

Kosaka, T., Miyajima, A., Takayama, E., Kikuchi, E., Nakashima, J., Ohigashi, T., et al. (2007). Angiotensin II type 1 receptor antagonist as an angiogenic inhibitor in prostate cancer. *Prostate*, *67*, 41–49.

Kosugi, M., Miyajima, A., Kikuchi, E., Horiguchi, Y., & Murai, M. (2006). Angiotensin II type 1 receptor antagonist candesartan as an angiogenic inhibitor in a xenograft model of bladder cancer. *Clinical Cancer Research*, *12*, 2888–2893.

Li, Y., & Sarkar, F. H. (2002). Inhibition of nuclear factor κB activation in PC-3 cells by genistein is mediated via Akt signaling pathway. *Clinical Cancer Research*, *8*, 2369–2377.

Lin, H. S., Chean, C. S., Ng, Y. Y., Chan, S. Y., & Ho, P. C. (2000). 2-Hydroxypropyl-beta-cyclodextrin increases aqueous solubility and photostability of all-trans-retinoic acid. *Journal of Clinical Pharmacy and Therapeutics*, *25*, 265–269.

Madan, J., Baruah, B., Nagaraju, M., Abdalla, M. O., Yates, C., Turner, T., et al. (2012). Molecular cycloencapsulation augments solubility and improves therapeutic index of brominated noscapine in prostate cancer cells. *Molecular Pharmaceutics*, *9*, 1470–1480.

Madan, J., Dhiman, N., Parmar, V. K., Sardana, S., Bharatam, P. V., Aneja, R., et al. (2010). Inclusion complexes of noscapine in beta-cyclodextrin offer better solubility and improved pharmacokinetics. *Cancer Chemotherapy and Pharmacology*, *65*, 537–548.

Marasini, N., Tran, T. H., Poudel, B. K., Cho, H. J., Choi, Y. K., Chi, S. C., et al. (2013). Fabrication and evaluation of pH-modulated solid dispersion for telmisartan by spray-drying technique. *International Journal of Pharmaceutics*, *441*, 424–432.

Mark, P., & Nilsson, L. (2001). Structure and dynamics of the TIP3P, SPC, and SPC/E water models at 298 K. *Journal of Physical Chemistry A*, *105*, 9954–9960.

Matsuyama, M., Funao, K., Kuratsukuri, K., Tanaka, T., Kawahito, Y., Sano, H., et al. (2010). Telmisartan inhibits human urological cancer cell growth through early apoptosis. *Experimental and Therapeutic Medicine*, *1*, 301–306.

McGann, M. R., Almond, H. R., Nicholls, A., Grant, J. A., & Brown, F. K. (2003). Gaussian docking functions. *Biopolymers*, *68*, 76–90.

McGaughey, G. B., Sheridan, R. P., Bayly, C. I., Culberson, J. C., Kreatsoulas, C., Lindsley, S., et al. (2007). Comparison of topological, shape, and docking methods in virtual screening. *Journal of Chemical Information and Modeling*, *47*, 1504–1519.

Miyajima, A., Kosaka, T., Asano, T., Asano, T., Seta, K., Kawai, T., et al. (2002). Angiotensin II type 1 antagonist prevents pulmonary metastasis of murine renal cancer by inhibiting tumor angiogenesis. *Cancer Research*, *62*, 4176–4179.

Mosmann, T. (1983). Rapid colorimetric assay for cellular growth and survival: Application to proliferation and cytotoxicity assays. *Journal of Immunological Methods*, *65*, 55–63.

Ozeki, K., Tanida, S., Morimoto, C., Inoue, Y., Mizoshita, T., Tsukamoto, H., et al. (2013). Telmisartan inhibits cell proliferation by blocking nuclear translocation of ProHB-EGF C-terminal fragment in colon cancer cells. *PLoS One*, *8*, e56770.

Rama Rao, K., Bhanumathi, N., Yadav, J. S., & Krishnaveni, N. S. (2004). *Inclusion complex of rifampicin, an anti-tubercular drug, with betacyclodextrin or 2-hydroxypropyl betacyclodextrin thereof*. United States Patent (US 2004/0082541 A1).

Sangalli, M. E., Zema, L., Maroni, A., Foppoli, A., Giordano, F., & Gazzaniga, A. (2001). Influence of betacyclodextrin on the release of poorly soluble drugs from inert and hydrophilic heterogeneous polymeric matrices. *Biomaterials*, *22*, 2647–2651.

Stangier, J., Schmid, J., Turck, D., Switek, H., Verhagen, A., Peeters, P. A., et al. (2000). Absorption, metabolism, and excretion of intravenously and orally administered [^{14}C] telmisartan in healthy volunteers. *Journal of Clinical Pharmacology*, *40*, 1312–1322.

Stella, V. J., & Rajewski, R. A. (1997). Cyclodextrins: Their future in drug formulation and delivery. *Pharmaceutical Research*, *14*, 556–567.

Wienen, W., Entzeroth, M., van Meel, J. C. A., Stangier, J., Busch, U., Ebner, T., et al. (2000). A review on telmisartan: A novel, long-acting angiotensin II-receptor antagonist. *Cardiovascular Drug Reviews*, *18*, 127–154.